

# Superconductivity in the vicinity of charge ordered state in organic conductor $\beta$ -(*meso*-DMBEDT-TTF)<sub>2</sub>PF<sub>6</sub>

Kazuyoshi YOSHIMI<sup>1</sup> \*, Masaaki NAKAMURA<sup>2</sup> and Hatsumi MORI<sup>1</sup>

<sup>1</sup>*Institute for Solid State Physics, University of Tokyo, Kashiwanoha, Kashiwa, Chiba 277-8581*

<sup>2</sup>*Department of Applied Physics, Faculty of Science, Tokyo University of Science, Kagurazaka, Shinjuku-ku, Tokyo 162-8601*

We study theoretically competition between the charge ordering and the superconductivity in the two-dimensional organic conductor  $\beta$ -(*meso*-DMBEDT-TTF)<sub>2</sub>PF<sub>6</sub>. We analyze the extended Hubbard model on a weakly-dimerized lattice based on the random phase approximation and Eliashberg equations. We found the reentrant behavior of the checkerboard-type charge-ordered phase in the phase diagram, and the triplet superconductivity due to the charge fluctuation in the neighboring region. In low temperatures, the singlet superconductivity also appears due to the enhancement of the spin fluctuation.

**KEYWORDS:** organic conductor,  $\beta$ -(*meso*-DMBEDT-TTF)<sub>2</sub>PF<sub>6</sub>, superconductivity, charge ordering, random phase approximation, Eliashberg equation, charge fluctuation

## 1. Introduction

Organic conductors have attracted attention for many years. About two decades ago, superconductivity was found in the low dimensional organic conductor (TMTSF)<sub>2</sub>PF<sub>6</sub> at the critical temperature  $T_c \approx 0.9$  K under the pressure  $P \approx 12$  kbar. Since then, about 130 kinds of organic superconductors have been discovered. It is notable that BEDT-TTF salts (ET salts) are about 50 kinds of them.<sup>1,2</sup> The ET salts are mainly quasi-two-dimensional (2D) conductors with 3/4-filled  $\pi$  band of the donor molecules. These materials exhibit very interesting electronic properties such as superconductivity, magnetism and charge ordering.

For example,  $\kappa$ -(ET)<sub>2</sub>X salts show superconducting (SC) transitions next to the antiferromagnetic state in the ( $P, T$ ) phase diagram. The theoretical calculations based on the half-filled extended Hubbard model where the strong dimerization is assumed show that this superconductivity is mediated by antiferromagnetic spin fluctuation.<sup>3-6</sup> In  $\alpha$ -(ET)<sub>2</sub>I<sub>3</sub> salt, there are several theoretical works for the superconductivity in the presence of a charge ordering by the random phase approximation (RPA).<sup>7,8</sup> In this case, the SC state is also considered to be mediated by the antiferromagnetic spin fluctuation. For  $\theta$ -(ET)<sub>2</sub>X salts where the various charge-ordered (CO) states are observed, there are several theoretical works on the CO states by the mean field theory.<sup>9,10</sup> The superconductivity of this material is explained that it is induced by both the spin and the charge fluctuations.<sup>11</sup>

---

\*E-mail address: yoshimi@issp.u-tokyo.ac.jp

In this paper, we focus on  $\beta$ -(*meso*-DMBEDT-TTF)<sub>2</sub>PF<sub>6</sub> salt ( $\beta$ -(DMeET)<sub>2</sub>PF<sub>6</sub> salt) which has been recently synthesized and investigated by Kimura and Mori *et al.*<sup>12–14</sup> The conduction layer of this material consists of weakly dimerized two molecules per a unit cell with the 3/4-filled band. This salt shows the metal-insulator (MI) transition at  $T_{\text{MI}} \approx 90$  K without the anomaly of the magnetic susceptibility around  $T_{\text{MI}}$ . The insulating state exhibits the checkerboard-type charge ordering (see Fig.1(b)) where the charge disproportion occurs within the dimer unit. Estimating the nearest neighbor Coulomb interaction by the point charge approximation, it is reported that the checkerboard type charge ordering cannot be explained, so that the effective molecular size and the electron-phonon interaction should be taken into account.<sup>12</sup> The most remarkable point is that the SC state of  $\beta$ -(DMeET)<sub>2</sub>PF<sub>6</sub> is next to the CO state in the  $(P, T)$  phase diagram, with the critical temperature  $T_c \approx 4$  K under the pressure  $P \approx 4$  kbar.<sup>13,14</sup>  $T_c$  decreases with increasing the magnetic field, and the superconducting transition is completely suppressed above 4 T down to 0.5 K.

It is well known that SC transitions often appear next to the magnetic ordered region of the  $(P, T)$  phase diagram not only in organics but also in heavy fermion systems.<sup>15–17</sup> This has been considered as a typical character of superconductivity with magnetically mediated pairing mechanism. Therefore, the fact that superconductivity appeared in the neighbor of the CO region is not only rare for organic conductors, but also important for possibilities of the superconductivity mediated by the charge fluctuation. Recently, SC state appeared in the neighboring region of the CO state is also found in  $\beta$ -vanadium bronze,<sup>18</sup> but no theoretical studies have been carried out.

From the above background, we study  $\beta$ -(DMeET)<sub>2</sub>PF<sub>6</sub> in the following two point of views: i) how the checkerboard-type charge ordering is stabilized in the weakly dimerized organic system. ii) how the SC region appears in the neighbor of the CO region from the metallic state.

The rest of this paper is organized as follows. In Sec. 2, we formulate susceptibilities and Eliashberg equations based on the RPA for the weakly dimerized 2D system. In Sec. 3, we determine appropriate parameter set of the model, and present results of the numerical analysis. Finally, summary and discussion are given in Sec. 4.

## 2. Formulation

In this section, we perform the analysis for the Hubbard-type model based on the random phase approximation following Kobayashi *et al.*<sup>7,8</sup> Throughout this paper we set  $k_B = \hbar = 1$ .

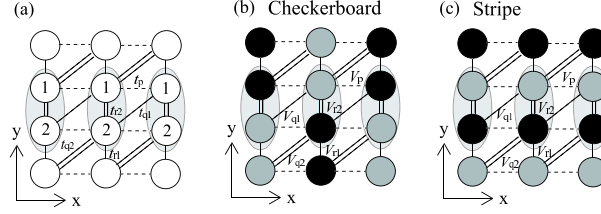


Fig. 1. (a) Model of the conduction layer for  $\beta$ -(DMeET) $_2$ PF $_6$  salt. The unit cell contains two molecules labeled by 1,2 with transfer integrals:  $t_{r1}, t_{r2}, t_{q1}, t_{q2}$  and  $t_p$ . We also introduce corresponding nearest neighbor Coulomb interactions:  $V_{r1}, V_{r2}, V_{q1}, V_{q2}$  and  $V_p$ . Two candidates of the charge ordered states in the present analysis, (b) the checkerboard and (c) the stripe type CO states, respectively. The black and gray molecules are in charge-rich and poor states.

## 2.1 Model

We apply the extended Hubbard model on the two-dimensional (2D) lattice (see Fig. 1 (a)),

$$\mathcal{H} = \mathcal{H}_t + \mathcal{H}_U + \mathcal{H}_V, \quad (1)$$

$$\mathcal{H}_t = \sum_{\langle i\alpha; j\beta \rangle} \sum_{\sigma} (t_{i\alpha; j\beta} c_{i\alpha\sigma}^{\dagger} c_{j\beta\sigma} + \text{H.c.}), \quad (2)$$

$$\mathcal{H}_U = \sum_{i\alpha} U_{\alpha} n_{i\alpha\uparrow} n_{i\alpha\downarrow}, \quad (3)$$

$$\mathcal{H}_V = \sum_{\langle i\alpha; j\beta \rangle} \sum_{\sigma\sigma'} V_{i\alpha; j\beta} n_{i\alpha\sigma} n_{j\beta\sigma'}, \quad (4)$$

where  $i, j$  ( $\in 1, \dots, N_L$ ) denote the lattice points of the 2D square lattice, and  $\alpha, \beta$  ( $\in 1, 2$ ) specify molecules in the unit cell.  $c_{i\alpha\sigma}^{\dagger}$  ( $c_{i\alpha\sigma}$ ) is the creation (annihilation) operator for an electron with spin  $\sigma$  ( $=\uparrow, \downarrow$ ).  $\langle i\alpha; j\beta \rangle$  represents a bond pair between the nearest neighbor sites.  $t_{i\alpha; j\beta}$  denotes the transfer energy between sites  $(i, \alpha)$  and  $(j, \beta)$ .  $\mathcal{H}_U$  and  $\mathcal{H}_V$  denote repulsive interactions where  $U_{\alpha}$  and  $V_{\alpha\beta}$  are the coupling for the on-site and those for the nearest neighbor sites, respectively. By using the Fourier transformation,

$$c_{i\alpha\sigma} = \frac{1}{\sqrt{N_L}} \sum_{\mathbf{k}} e^{i\mathbf{k} \cdot \mathbf{r}_i} c_{\mathbf{k}, \alpha, \sigma}, \quad (5)$$

eq. (1) is rewritten as

$$\begin{aligned} \mathcal{H} = & \sum_{\mathbf{k}\alpha\beta\sigma} (\varepsilon_{\alpha\beta}(\mathbf{k}) c_{\mathbf{k}\alpha\sigma}^{\dagger} c_{\mathbf{k}\beta\sigma} + \text{H.c.}) \\ & + \frac{1}{N_L} \sum_{\mathbf{k}\mathbf{k}'\mathbf{q}\alpha} U_{\alpha} c_{\mathbf{k}+\mathbf{q}, \alpha, \uparrow}^{\dagger} c_{\mathbf{k}, \alpha, \uparrow} c_{\mathbf{k}'-\mathbf{q}, \alpha, \downarrow}^{\dagger} c_{\mathbf{k}', \alpha, \downarrow} \\ & + \frac{1}{2N_L} \sum_{\mathbf{k}\mathbf{k}'\mathbf{q}\alpha\beta\sigma\sigma'} V_{\alpha\beta}(\mathbf{q}) c_{\mathbf{k}+\mathbf{q}, \alpha, \sigma}^{\dagger} c_{\mathbf{k}, \alpha, \sigma} c_{\mathbf{k}'-\mathbf{q}, \beta, \sigma'}^{\dagger} c_{\mathbf{k}', \beta, \sigma'} \end{aligned} \quad (6)$$

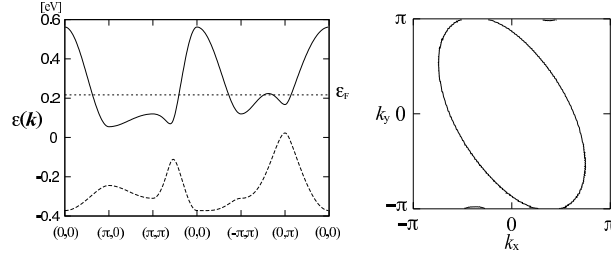


Fig. 2. Energy band spectra  $\xi_1$  and  $\xi_2$  of eq. (13) and the Fermi surface.

where the parameters in eq. (6) are taken as,  $\varepsilon_{11} = \varepsilon_{22}$ ,  $\varepsilon_{12} = \varepsilon_{21}^*$ ,  $V_{11} = V_{22}$ ,  $V_{12} = V_{21}^*$ . Then the transfer energies are

$$\varepsilon_{11}(\mathbf{k}) = 2t_p \cos k_x, \quad (7)$$

$$\varepsilon_{12}(\mathbf{k}) = t_{r1}e^{-ik_y} + t_{r2} + t_{q1}e^{ik_x} + t_{q2}e^{-i(k_x+k_y)}. \quad (8)$$

The long range Coulomb interactions become

$$V_{11}(\mathbf{q}) = 2V_p \cos q_x, \quad (9)$$

$$V_{12}(\mathbf{q}) = V_{r1}e^{-iq_y} + V_{r2} + V_{q1}e^{iq_x} + V_{q2}e^{-i(q_x+q_y)}. \quad (10)$$

Applying the mean field approximation, the Hamiltonian is given by

$$\mathcal{H}_{\text{MF}} = \sum_{\mathbf{k}\alpha\beta\sigma} \tilde{\varepsilon}_{\alpha\beta\sigma}(\mathbf{k}) c_{\mathbf{k}\alpha\sigma}^\dagger c_{\mathbf{k}\beta\sigma} + \text{const.}, \quad (11)$$

$$\tilde{\varepsilon}_{\alpha\beta\sigma}(\mathbf{k}) = \varepsilon_{\alpha\beta}(\mathbf{k}) + \delta_{\alpha\beta} \left[ U_\alpha \langle n_{\alpha\bar{\sigma}} \rangle + \sum_{\beta'\sigma'} V_{\alpha\beta'} \langle n_{\beta'\sigma'} \rangle \right], \quad (12)$$

where  $\bar{\sigma}$  denotes the opposite spin of  $\sigma$ . In this approximation, we ignore the Fock term ( $\langle c_{i\alpha}^\dagger c_{j\beta} \rangle \simeq 0$ ) and assume the uniform ground state:  $\langle n_{\alpha\sigma} \rangle = 3/4$ . The Hamiltonian is diagonalized as

$$E_{\text{MF}} = \sum_{\mathbf{k}\alpha\gamma\sigma} \xi_{\gamma\sigma}(\mathbf{k}) d_{\alpha\gamma\sigma}^*(\mathbf{k}) d_{\alpha\gamma\sigma}(\mathbf{k}), \quad (13)$$

where  $\xi_1(\mathbf{k}) > \xi_2(\mathbf{k})$  ( see Fig. 2 ).  $d_{\alpha\gamma\sigma}(\mathbf{k})$  is the element of unitary matrix obtained by diagonalization of eq. (11). Then,  $\langle n_{\alpha\sigma} \rangle$  is given as

$$\langle n_{\alpha\sigma} \rangle = \sum_{\gamma=1}^2 \frac{d_{\alpha\gamma\sigma}^*(\mathbf{k}) d_{\alpha\gamma\sigma}(\mathbf{k})}{\exp [(\xi_{\gamma\sigma}(\mathbf{k}) - \mu)/T] + 1}, \quad (14)$$

where  $\mu$  is the chemical potential determined by the condition of 3/4-filling:  $\frac{1}{2} \sum_{\alpha\sigma} \langle n_{\alpha\sigma} \rangle = \frac{3}{2}$ .

## 2.2 Charge and spin susceptibilities

We define matrices of susceptibility as

$$(X_{\sigma\sigma'}(\mathbf{q}, i\omega_n))_{\alpha\beta} \equiv \frac{1}{N_L} \int_0^{1/T} d\tau e^{i\omega_n \tau} \langle n_{\alpha\sigma}(\mathbf{q})(\tau) n_{\beta\sigma'}(-\mathbf{q})(0) \rangle, \quad (15)$$

where  $\omega_l$  is the Matsubara frequency for bosons.<sup>7</sup>  $\tau$  is the imaginary time. The density operator  $n_{\alpha,\sigma}(\mathbf{q})$  is given by

$$n_{\alpha,\sigma}(\mathbf{q}) = \sum_{\mathbf{k}} c_{\mathbf{k},\alpha,\sigma}^\dagger c_{\mathbf{k}+\mathbf{q},\alpha,\sigma}. \quad (16)$$

The charge susceptibility  $\hat{X}^c$  and the spin susceptibility for the easy axis  $\hat{X}^s$  are given by

$$\hat{X}_{\alpha\beta}^c = \frac{1}{2}(\hat{X}_{\uparrow\uparrow} + \hat{X}_{\downarrow\uparrow} + \hat{X}_{\uparrow\downarrow} + \hat{X}_{\downarrow\downarrow})_{\alpha\beta}, \quad (17)$$

$$\hat{X}_{\alpha\beta}^s = \frac{1}{2}(\hat{X}_{\uparrow\uparrow} - \hat{X}_{\downarrow\uparrow} - \hat{X}_{\uparrow\downarrow} + \hat{X}_{\downarrow\downarrow})_{\alpha\beta}. \quad (18)$$

Applying the random phase approximation and ignoring the Fock term, we obtain

$$\begin{aligned} \hat{X}_{\sigma\sigma} &= [I + \hat{X}^{(0)} \hat{V}^{(1)} - \hat{X}^{(0)} \hat{V}^{(2)} (I + \hat{X}^{(0)} \hat{V}^{(1)})^{-1} \\ &\quad \times \hat{X}^{(0)} \hat{V}^{(2)}]^{-1} \hat{X}^{(0)}, \end{aligned} \quad (19)$$

$$\begin{aligned} \hat{X}_{\bar{\sigma}\sigma} &= -(I + \hat{X}^{(0)} \hat{V}^{(1)})^{-1} \hat{X}^{(0)} \hat{V}^{(2)} [I + \hat{X}^{(0)} \hat{V}^{(1)} \\ &\quad - \hat{X}^{(0)} \hat{V}^{(2)} (I + \hat{X}^{(0)} \hat{V}^{(1)})^{-1} \hat{X}^{(0)} \hat{V}^{(2)}]^{-1} \hat{X}^{(0)}. \end{aligned} \quad (20)$$

$\hat{V}^{(1)}$  and  $\hat{V}^{(2)}$  are given by

$$\hat{V}^{(1)} = \hat{V} + \hat{U}, \quad \hat{V}^{(2)} = \hat{V} \quad (21)$$

where  $\hat{V}$  and  $\hat{U}$  are defined as

$$\hat{V} = \begin{pmatrix} V_{11}(\mathbf{q}) & V_{12}(\mathbf{q}) \\ V_{21}(\mathbf{q}) & V_{22}(\mathbf{q}) \end{pmatrix}, \quad \hat{U} = \begin{pmatrix} U & 0 \\ 0 & U \end{pmatrix}. \quad (22)$$

In this case, we treat mainly the nonmagnetic state, i.e.,  $X_{\uparrow\uparrow} = X_{\downarrow\downarrow}$ ,  $X_{\uparrow\downarrow} = X_{\downarrow\uparrow}$ . Then  $\hat{X}^c$  and  $\hat{X}^s$  are given by

$$\begin{aligned} \hat{X}^c &= \hat{X}_{\uparrow\uparrow} + \hat{X}_{\uparrow\downarrow} \\ &= (\hat{I} + \hat{X}^{(0)}(\hat{U} + 2\hat{V}))^{-1} \hat{X}^{(0)}, \end{aligned} \quad (23)$$

$$\begin{aligned} \hat{X}^s &= \hat{X}_{\uparrow\uparrow} - \hat{X}_{\uparrow\downarrow} \\ &= (\hat{I} - \hat{X}^{(0)}\hat{U})^{-1} \hat{X}^{(0)}, \end{aligned} \quad (24)$$

where  $\hat{X}^c$  and  $\hat{X}^s$  are hermitian matrices. The irreducible susceptibility  $\hat{X}^{(0)}$  is

$$X_{\alpha\beta}^{(0)}(\mathbf{q}, i\omega_n) = -\frac{T}{N_L} \sum_{\mathbf{k}, n} G_{\alpha\beta}^{(0)}(\mathbf{k} + \mathbf{q}, i\omega_m + i\epsilon_n) G_{\beta\alpha}^{(0)}(\mathbf{k}, i\epsilon_n)$$

where  $\epsilon_n$  denotes the Matsubara frequency for fermions.  $G_{\alpha\beta}^{(0)}(\mathbf{k}, i\omega_n)$  is the single particle Green function given by

$$G_{\alpha\beta}^{(0)}(\mathbf{k}, i\epsilon_n) = \sum_{\gamma=1}^2 \frac{d_{\alpha\gamma}(\mathbf{k}) d_{\beta\gamma}^*(\mathbf{k})}{i\epsilon_n - \xi_{\gamma}(\mathbf{k}) + \mu}, \quad (25)$$

where  $\xi_{\gamma}(\mathbf{k})$  and  $d_{\alpha,\gamma}(\mathbf{k})$  are defined in eq. (13).

Now, we introduce the linear combinations of the density operators as

$$n_{\pm}(\mathbf{q}) = \frac{1}{\sqrt{2}} (n_1(\mathbf{q}) \pm n_2(\mathbf{q})). \quad (26)$$

Then replacing the original density operators in eq. (15), and taking account the symmetry in the unit cell, the corresponding charge ( $\nu = c$ ) and spin ( $\nu = s$ ) susceptibilities are given by

$$\begin{aligned} \hat{X}_{\pm}^{\nu} &= \frac{1}{2} (\hat{X}_{11}^{\nu} \pm \hat{X}_{21}^{\nu} \pm \hat{X}_{12}^{\nu} + \hat{X}_{22}^{\nu}) \\ &= \hat{X}_{11}^{\nu} \pm \text{Re } \hat{X}_{12}^{\nu}. \end{aligned} \quad (27)$$

The stability of the CO states in the present analysis (see Fig.1 (b), (c)) is given by divergence of  $\hat{X}_{-}^c$ .

### 2.3 Pairing interactions and Eliashberg equations

The superconducting transition point is determined by the Eliashberg equation. The linearized Eliashberg equation for the singlet SC state is given by

$$\begin{aligned} \lambda_S \Sigma_{\alpha\sigma;\beta\bar{\sigma}}^a(\mathbf{k}) &= -\frac{1}{N_L} \sum_{\mathbf{k}', n', \alpha', \beta'} P_{\alpha\sigma;\beta\bar{\sigma}}^S(\mathbf{k} - \mathbf{k}') \\ &\times G_{\alpha\alpha'}^{(0)}(\mathbf{k}', i\epsilon_{n'}) G_{\beta\beta'}^{(0)}(-\mathbf{k}', -i\epsilon_{n'}) \Sigma_{\alpha'\sigma;\beta'\bar{\sigma}}^a(\mathbf{k}'), \end{aligned} \quad (28)$$

with the pairing interaction,

$$\hat{P}^S = \hat{U} + \hat{V} + \frac{3}{2} \hat{U} \hat{X}^s \hat{U} - \frac{1}{2} (\hat{U} + 2\hat{V}) \hat{X}^c (\hat{U} + 2\hat{V}), \quad (29)$$

where  $\hat{X}^c$  and  $\hat{X}^s$  are the susceptibility matrices given in eqs.(23) and (24). In eq. (28),  $\Sigma_{\alpha\sigma;\beta\bar{\sigma}}^a(\mathbf{k})$  is the anomalous self-energy with the space inversion symmetry  $\Sigma_{\alpha\sigma;\beta\bar{\sigma}}^a(\mathbf{k}) = \Sigma_{\beta\bar{\sigma};\alpha\bar{\sigma}}^a(-\mathbf{k})$ . Here we neglect the dependence of the Matsubara frequency in  $\Sigma_{\alpha\sigma;\beta\bar{\sigma}}^a(\mathbf{k})$ , since such a treatment is valid for the weak coupling case.<sup>11</sup> In eq. (28),  $\lambda_S = 1$  corresponds to the superconducting transition point.

Similarly, the linearized Eliashberg equation for the triplet SC state is obtained as

$$\begin{aligned} \lambda_T \Sigma_{\alpha\sigma;\beta\sigma}^a(\mathbf{k}) &= -\frac{1}{N_L} \sum_{\mathbf{k}', n', \alpha', \beta'} P_{\alpha\sigma;\beta\sigma}^T(\mathbf{k} - \mathbf{k}') \\ &\times G_{\alpha\alpha'}^{(0)}(\mathbf{k}', i\epsilon_{n'}) G_{\beta\beta'}^{(0)}(-\mathbf{k}', -i\epsilon_{n'}) \Sigma_{\alpha'\sigma;\beta'\sigma}^a(\mathbf{k}'), \end{aligned} \quad (30)$$

with the paring interaction,

$$\hat{P}^T = \hat{V} - \frac{1}{2}\hat{U}\hat{X}^s\hat{U} - \frac{1}{2}(\hat{U} + 2\hat{V})\hat{X}^c(\hat{U} + 2\hat{V}). \quad (31)$$

In order to confirm the relevant part of the effective interaction for the singlet state, we divide the paring interaction into the following two parts,

$$\hat{P}^c = \hat{V} - \frac{1}{2}(\hat{U} + 2\hat{V})\hat{X}^c(\hat{U} + 2\hat{V}), \quad (32)$$

$$\hat{P}^s = \hat{U} + \frac{3}{2}\hat{U}\hat{X}^s\hat{U}. \quad (33)$$

In the present linearized Eliashberg equations, the amplitude of the anomalous energies can be chosen arbitrary, so that we calculate the quasi-particle bands just below the SC transition temperature. The quasi-particle bands is obtained by the following Hamiltonian,

$$\begin{aligned} \mathcal{H}_{\text{MF}}^{\text{SC}} = & \mathcal{H}_{\text{MF}} - \mu \sum_{\mathbf{k}} \sum_{\sigma} \sum_{\alpha} c_{\mathbf{k}\alpha\sigma}^{\dagger} c_{\mathbf{k}\alpha\sigma} \\ & + \lambda (\sum_{\alpha\beta}^{\text{a}}(\mathbf{k}) c_{\mathbf{k}\alpha\sigma}^{\dagger} c_{-\mathbf{k}\beta\sigma_1}^{\dagger} + \sum_{\alpha\beta}^{\text{a}*}(\mathbf{k}) c_{-\mathbf{k}\beta\sigma_1} c_{\mathbf{k}\alpha\sigma}) \end{aligned} \quad (34)$$

where  $\sigma_1 = \bar{\sigma}$  ( $\sigma_1 = \sigma$ ) for the singlet (triplet) SC state.

### 3. Numerical Results

Since there are a lot of parameters in the present model, we select a set of parameters in the following way. First, we fix the transfer integrals calculated by the extended Hückel method based upon the crystal structure analysis:  $t_{r1} = -0.0824$ ,  $t_{r2} = -0.226$ ,  $t_p = 0.0475$ ,  $t_{q1} = -0.0438$  and  $t_{q2} = -0.115$  [eV].<sup>13</sup> In this case, we do not consider explicit pressure dependence of the parameters. Next, we determine the value of the on-site Coulomb energy  $U$  which becomes the ground state nonmagnetic. Then we determine the value of the nearest neighbor interactions  $V$  which stabilize the checkerboard type CO state. We use the unit for the energies as [eV]. Finally, we determine the phase diagram of this model.

#### 3.1 Nonmagnetic state

To obtain the phase diagram in the  $(U, T)$  plane (Fig. 3(a)), we calculate  $X_+^s$  which is larger than  $X_-^s$ . Figure 3(b) shows the momentum dependence of the spin susceptibilities  $X_{\pm}^s$ , at  $T = 0.1$ . When the system is dimerized, the exchange coupling  $J = \frac{4t^2}{U}$  becomes  $J_x > J_{xy} > J_y$ , where  $|t_x| = |t_p - t_{q1}/2| = 0.069 > |t_{xy}| = |t_{q2}|/2 = 0.056 > |t_y| = |t_{r1}/2| = 0.0412$ .<sup>2</sup> As a result,  $X_+^s$  becomes the largest at  $(\pi, 0)$ .  $\beta$ -(DMeET)<sub>2</sub>PF<sub>6</sub> is nonmagnetic. Therefore, we fix the on-site Coulomb interaction  $U$  at 0.4 [eV] in the following calculation where the spin density wave (SDW) does not appear.

#### 3.2 Charge ordered states

We investigate the combination of the nearest neighbor Coulomb interactions  $V$ , where the checkerboard type charge order is stabilized. First, we examine the charge order patterns

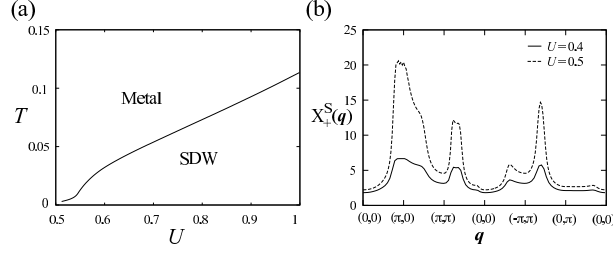


Fig. 3. (a) Phase diagram in the  $(U, T)$  plane. The solid line correspond to the phase boundary between the metallic and the SDW states. (b) Spin susceptibilities  $X_+^s(\mathbf{q})$  for  $U = 0.4$  and  $0.5$  at  $T = 0.01$ .

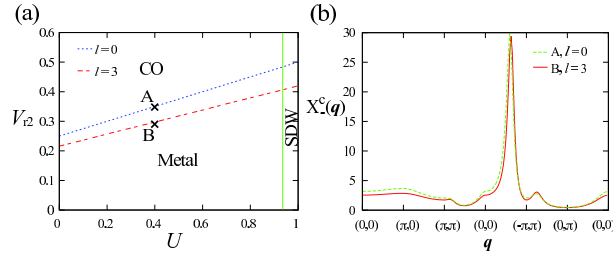


Fig. 4. (a) Phase diagram on  $(U, V_{r2})$  plane at  $T = 0.1$ . The dashed and the solid lines correspond to the CO and the SDW instabilities, respectively. (b) Charge susceptibilities  $X_-^c(\mathbf{q})$  for  $(V_{r2}, l) = (0.35, 0), (0.294, 3)$  at  $T = 0.1, U = 0.4$ .

by using the point charge approximation:  $V_i \propto \frac{1}{r_i}$ . Figure 4(a) shows the phase diagram on the  $(U, V_{r2})$  plane at  $T = 0.1$ .  $\hat{X}_-^c$  becomes larger in the intermediate region between  $(0, 0)$  and  $(-\pi, \pi)$  as shown in Fig. 4(b), therefore we find that this result does not accord with the experimental fact. Taking account of the effective molecular size  $l$ , the coulomb interaction in the dimer is given as  $V_{r2} \propto (r_{r2}^2 + l^2)^{-1/2}$ . It is reported that  $l \approx 3 \text{ \AA}$  is reasonable for the ET salt.<sup>19</sup> Therefore we fix  $l$  at  $3 \text{ \AA}$  and apply the point charge approximation for the other  $V$ s. Figure 4(a) shows  $(U, V_{r2})$ -phase diagram at  $T = 0.1$ . In the case of  $l = 3 \text{ \AA}$ , the CO instability occurs in the smaller  $V_{r2}$  than that of  $l = 0 \text{ \AA}$ . This indicates that the charge fluctuation becomes larger by taking account of the molecular size, because the difference between  $V_{r2}$  and another  $V$  is smaller. However, the critical point of  $X_-^c(\mathbf{q})$  does not change and we cannot obtain the checkerboard type charge ordering.

In order to stabilize the checkerboard type CO state, it is suitable to satisfy the following condition:  $(V_{r2}, V_p, V_{q2}) > (V_{r1}, V_{q1})$ . For simplicity, we assume only two sets of nearest neighbor interactions  $V_1 (= V_p = V_{q2})$  and  $V_2 (= V_{r1} = V_{q1})$ . As shown in Fig. 1(b),  $V_1$  is the interaction to induce the charge disproportion with the charge density in the unit cell:  $n_{i1} \neq n_{i2}$ .  $V_2$  is the interaction to favor the uniform charge density in the unit cell:  $n_{i1} = n_{i2}$ . We set  $V_{r2} = s_1 \times U$ ,  $V_1 = V_p = V_{q2} = s_2 \times V_{r2}$ ,  $V_2 = V_{r1} = V_{q1} = s_3 \times V_{r2}$ . For nonmagnetic



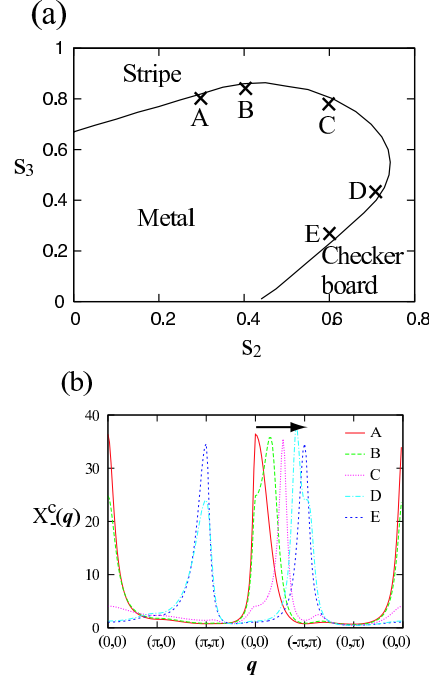


Fig. 5. (a) Phase diagram on  $(s_2, s_3)$  plane at  $T = 0.1, U = 0.4, V_{r2} = 0.8U$ . The solid line corresponds to the CO instability. (b) Charge susceptibilities  $X_c^c(\mathbf{q})$  for  $(s_2, s_3) = A(0.3, 0.8), B(0.4, 0.84), C(0.6, 0.78), D(0.7, 0.41)$  and  $E(0.6, 0.25)$  at  $T = 0.1, U = 0.4, V_{r2} = 0.8U$ . The arrow shows the shift of the peak of  $X_c^c(\mathbf{q})$  from  $(0, 0)$  to  $(\pi, \pi)$

states, we fix  $U = 0.4$  eV and  $V_{r2} = 0.8 \times U$  as shown in Fig. 3(a).

Figure 5 shows the phase diagram on the  $(s_2, s_3)$  plane. As shown in Fig. 5(b), a peak of  $X_c^c$  appears at  $(0, 0)$  in the stripe type CO phase (Fig. 1(c)), and  $(\pi, \pi)$  in the checkerboard type CO phase (Fig. 1(b)). The wave number for the peak of  $X_c^c$  changes continuously in the intermediate region between the stripe and the checkerboard type CO regimes. In the parameter region of the point charge approximation,  $s_2$  is nearly equal to  $s_3$ , but  $s_2$  should be sufficiently larger than  $s_3$  to realize the checkerboard type CO state. When we take account of the correspondence with the real material, it is suitable that the difference between  $s_2$  and  $s_3$  is small. Therefore, we set  $s_3 = 0.3$ .

Next, we examine the CO state by varying the temperature. The obtained phase diagram is shown in Fig. 6(a). There is a reentrant charge order transition as a function of temperature similar to the result of the extended Hubbard model in the 2D square lattice.<sup>20</sup> We consider that this reentrant behavior is due to the competition between the effect of  $V(\mathbf{q})$  and  $X^{(0)}(\mathbf{q})$ . At high temperatures, the peak of  $X_c^c$  is near  $(\pi, \pi)$ . This originates from the momentum dependence of  $V(\mathbf{q})$ . With decreasing temperatures, the momentum dependence of  $X^{(0)}(\mathbf{q})$  becomes large. Thus the peak of  $X_c^c(\mathbf{q})$  changes from  $(\pi, \pi)$  as shown in Fig. 6 (b).

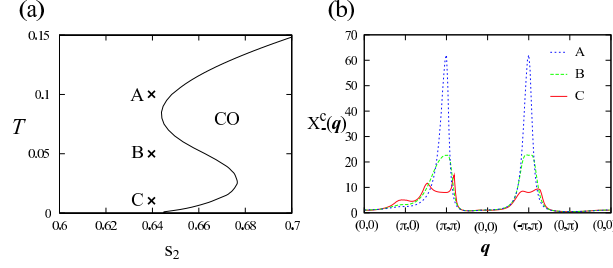


Fig. 6. (a) Phase diagram for the CO state on  $(s_2, T)$  plane at  $U = 0.4, V_{r2} = 0.8U, V_2 = 0.3V_{r2}$ . The solid line corresponds to the CO instability. (b) Charge susceptibilities  $X_-^c(\mathbf{q})$  for  $T =$  (A) 0.1, (B) 0.05 and (C) 0.01 at  $U = 0.4, V_{r2} = 0.8U, V_1 = 0.64V_{r2}$  and  $V_2 = 0.3V_{r2}$ .

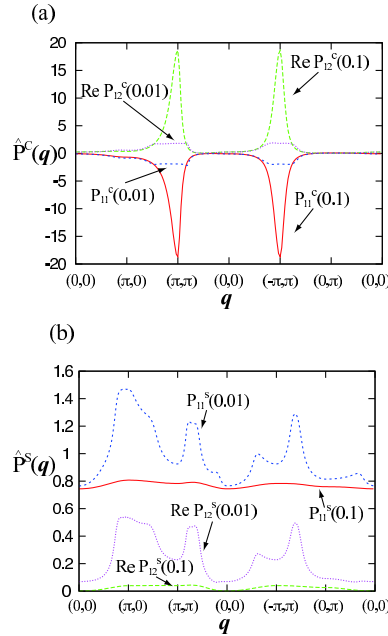


Fig. 7. Momentum dependence of the pairing interactions for the (a) charge [eq. (32)] and the (b) spin parts [eq. (33)],  $P_{\alpha\beta}^{c(s)}(T)$ , at  $U = 0.4, V_{r2} = 0.8U$  and  $V_2 = 0.3V_{r2}$ . We set  $s_2 = 0.64$  at  $T = 0.1$  and  $s_2 = 0.613$  at  $T = 0.01$ , respectively.

### 3.3 Pairing interactions and superconducting states

First, we examine the effect of  $\hat{P}^c$ . Figure 7(a) shows the momentum dependence of  $\hat{P}^c$ . At  $(s_2, T) = (0.64, 0.1)$ ,  $\hat{P}_{11}^c$  shows a negative peak at  $(\pi, \pi)$ , whereas  $\hat{P}_{12}^c$  shows a positive peak. This result is consistent with the appearance of the checkerboard-type charge ordering. The effective repulsive interaction is caused by the Coulomb interactions where  $V_{r2}$  and  $V_1$  are larger than  $V_2$ . On the other hand, the effective attractive interaction arises by other Coulomb interactions  $V_2$ . At  $(s_2, T) = (0.64, 0.01)$ , the peak of  $\hat{P}^c$  is suppressed and changes from  $(\pi, \pi)$ . We think it originates from the reentrant behavior of the CO.

The momentum dependence of  $P^s$  is determined by that of  $\hat{X}^{(0)}$ , because  $U$  does not

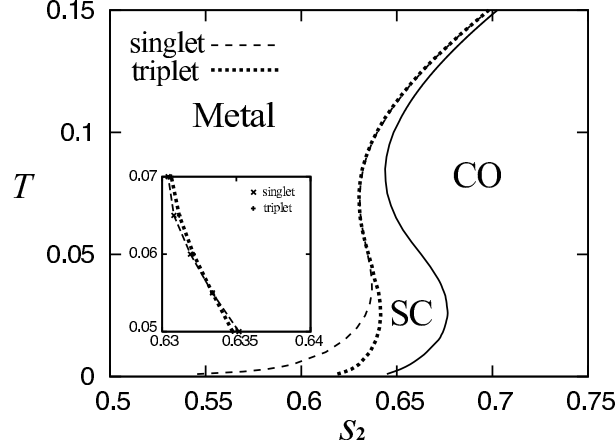


Fig. 8. Phase diagram on  $(s_2, T)$  plane at  $U = 0.4, V_{r2} = 0.8U, V_2 = 0.3V_{r2}$ . The solid line corresponds to the CO instability. Note that the superconducting (SC) region is overestimated in the present analysis for the high-temperature region. The inset shows the detail close to  $T = 0.06$  where the triplet SC state competes with the singlet SC state.

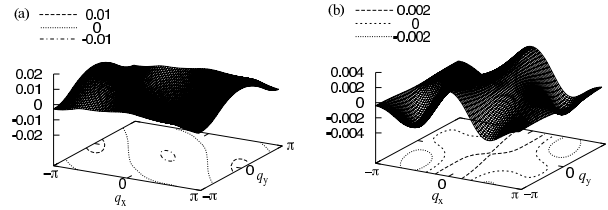


Fig. 9. The momentum dependence of the element of anomalous self-energy matrix  $\Sigma_{11}$  of the singlet SC state for (a)  $T=0.01, s_2=0.613$  and (b)  $T=0.1, s_2=0.64$ .

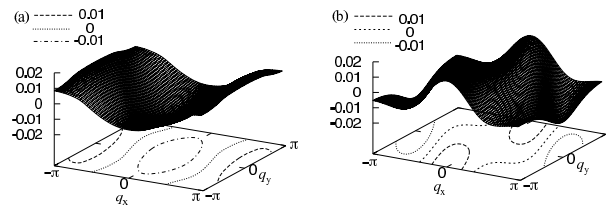


Fig. 10. The momentum dependence of the element of anomalous self-energy matrix  $\text{Re}\Sigma_{12}$  of the singlet SC state for (a)  $T=0.01, s_2=0.613$  and (b)  $T=0.1, s_2=0.64$ .

depend on the momentum. As shown in Fig. 7(b), the momentum dependence of  $P^s$  increases with lowering temperatures. It is notable that  $\hat{P}^c$  is much larger than  $\hat{P}^s$  at  $T = 0.1$  meaning that the SC state originates from the charge fluctuation. However, at  $T = 0.01$ , both  $\hat{P}^c$  and  $\hat{P}^s$  are the same order. Therefore we expect that the SC state in this region is caused by both the charge and the spin fluctuations.

In order to estimate the onset temperature for the SC states, we evaluate the linearized

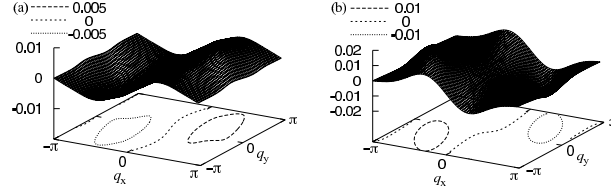


Fig. 11. The momentum dependence of the element of anomalous self-energy matrix  $\text{Im}\Sigma_{12}$  of the singlet SC state for (a)  $T=0.01$ ,  $s_2=0.613$  and (b)  $T=0.1$ ,  $s_2=0.64$ .

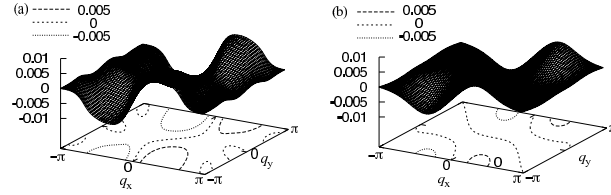


Fig. 12. The momentum dependence of the element of anomalous self-energy matrix  $\Sigma_{11}$  of the triplet SC state for (a)  $T=0.01$ ,  $s_2=0.636$  and (b)  $T=0.1$ ,  $s_2=0.64$ .

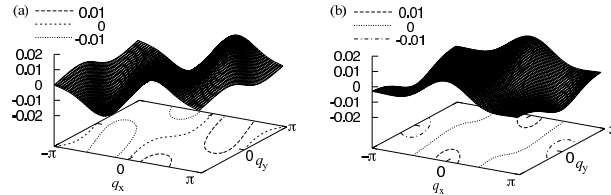


Fig. 13. The momentum dependence of the element of anomalous self-energy matrix (a)  $\text{Re}\Sigma_{12}$  and (b)  $\text{Im}\Sigma_{12}$  of the triplet SC state for  $T=0.1$ ,  $s_2=0.64$ .

Eliashberg equations eqs. (28), (30). Then we obtain the phase diagram on the  $(s_2, T)$  plane as shown in Fig. 8, the singlet SC state competes with the triplet SC state for  $0.05 < T$ , but the singlet SC transition occurs first for  $T < 0.05$ . This means that an incommensurate CO phase is developed as lowering temperatures.

As shown in Figs. 9 and 10, the anomalous self-energy of the singlet SC state strongly depends on the temperature. For the singlet SC state at  $T = 0.1$ ,  $\text{Re}\Sigma_{12}$  is larger than  $\Sigma_{11}$ . This indicates that  $\text{Re}\Sigma_{12}$  contributes mainly to the SC state at  $T = 0.1$ . On the other hand,  $\text{Re}\Sigma_{12}$  is the same order of  $\Sigma_{11}$ . This indicates that both  $\Sigma_{11}$  and  $\text{Re}\Sigma_{12}$  contribute to the SC state at  $T = 0.01$ . As mentioned above, the spin fluctuation increases with lowering temperatures (Fig. 7) and  $P^s$  is the same order of  $P^c$  at  $T = 0.01$ . The pairing interactions do not have a special peak, since the anomalous self-energies are broad.

The anomalous self-energy of the triplet SC does not depend much on the temperature as shown in Fig. 12.  $\text{Re}P_{12}^s$  is smaller than  $P_{11}^s$ . It follows from eq. (31) that the total pairing

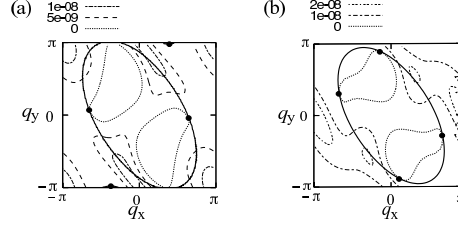


Fig. 14. The gap of the singlet SC state from the quasi-particle band of the noninteracting case at (a)  $T = 0.01$  with  $s_2 = 0.64$  and (b)  $T = 0.1$  with  $s_2 = 0.613$ . The solid and dashed line correspond to the Fermi line and the gap, respectively.

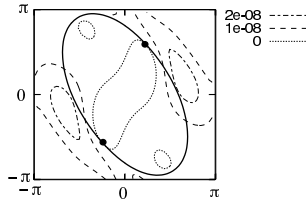


Fig. 15. The gap of the triplet SC state from the quasi-particle band of the noninteracting case at  $T = 0.1$  with  $s_2 = 0.613$ . The solid and dashed line correspond to the Fermi line and the gap, respectively.

interaction of the triplet SC state is given by  $\hat{P}^T = \hat{P}^c - \frac{1}{3}(\hat{P}^s - \hat{U})$ . This indicates that the triplet SC state is less affected by the spin fluctuation than the singlet SC state. Therefore, we consider that the triplet SC state is mainly induced by the charge fluctuation. It is reasonable that the triplet SC state appears near the CO state.

Finally, we determine the symmetry of the order parameters by calculating the quasi-particle bands and count the numbers of zero points of gaps at the Fermi surface. We analyze eq. (34) as  $\lambda \ll 1$ : we set  $\lambda = 10^{-4}$  in this calculation, since the SC gap is regarded as infinitesimal. It is shown that the singlet SC state has 4 nodes as seen from Fig. 14. On the other hand, the triplet SC state has 2 nodes as shown in Fig. 15. In this result, however, we found a pathological behavior of the triplet gap which does not vanish at the center of the momentum space  $\mathbf{k} = (0, 0)$ , even though it satisfies the fermion antisymmetry. In fact, in the present analysis, we cannot classify the singlet and triplet gaps as the parity in the momentum space. This reason is explained as follows: The symmetry of the singlet (triplet) state is given as  $\Sigma_{\alpha\beta}^a(\mathbf{k}) = \pm \Sigma_{\beta\alpha}^a(-\mathbf{k})$ , so that  $\Sigma_{\alpha\beta}^a(\mathbf{k}) = \pm \Sigma_{\alpha\beta}^a(-\mathbf{k})$  is not satisfied in general for  $\alpha \neq \beta$ . Therefore, the singlet (triplet) gap may include the parity-odd (-even) off-diagonal components as shown in Fig. 11 (Fig. 13). In spite of this extra freedoms, the number of nodes coincides with the usual singlet- and triplet-gap properties. The explanation of this fact remains a future problem.

#### 4. Summary and Discussion

We have theoretically examined the CO and the SC states of  $\beta$ -(DMeET)<sub>2</sub>PF<sub>6</sub>. We have analyzed the extended Hubbard model including the nearest Coulomb interactions in the weakly dimerized lattice. Applying the RPA, we choose the suitable parameters realizing the checkerboard type CO state under the nonmagnetic state. The CO phase shows reentrant behavior as a function of the temperature. We consider that this behavior originates from the competition between the wave vector dependence of  $V$  and the nesting effect of the charge susceptibility.

Using the pairing interactions induced by the charge and spin fluctuations in terms of the RPA, we have estimated the onset temperature of the SC state near the CO instability by the linearized Eliashberg equations. The triplet SC state is stabilized around the region of the CO instability which originates from the wave vector dependence of  $V(\mathbf{q})$ . On the other hand, the singlet SC state is stabilized near the region of the CO instability which originates from the nesting vector of the Fermi surface.

The determination of parameters of the present model has been carried out to realize the checkerboard type CO state under the nonmagnetic state, comparing with the experimental result. However, values of these parameters are much different from those expected by the point charge approximation, even taking account of the effective molecular size. This suggests that the electron-phonon interaction due to the lattice distortion might be important to understand the checkerboard type CO state.

In this paper, we have assumed that the CO state is an insulating state. There is a possibility, however, that the CO state is a metallic state due to existence of the hole and the electron pocket in the Fermi surface, and a SC state coexists with the CO state. This scenario was asserted to explain the superconductivity of  $\alpha$ -(ET)<sub>2</sub>I<sub>3</sub> salt under uniaxial pressure.<sup>7,8</sup> Actually, the temperature and the pressure dependences of the resistivity in certain parameter regions seem to behave similarly in these two systems.<sup>13,21</sup> If such a metallic state is realized, the phase diagram of Fig. 8 may be modified so that a different type of SC state appears in the CO region, but the SC states obtained in the present analysis remain to be unchanged.

#### 5. Acknowledgements

The authors thank Y. Suzumura and A. Kobayashi for discussion and many helpful suggestions. We acknowledge T. Kato for helpful comments on the mean field calculation, and Y. Tanaka for discussion about the numerical analysis of the linearized Eliashberg equations. We are also grateful to H. Fukuyama and C. Ishii for useful comments. One of the authors (M. N.) is partly supported by the Grant-in-Aid for scientific research of the Ministry of Education, Science, Sports and Culture of Japan.

## References

- 1) T. Ishiguro, K. Yamaji and G. Saito: Organic Superconductors (Springer-Verlag, Berlin, 1998) 2nd ed.
- 2) H. Seo, C. Hotta and H. Fukuyama: Chem. Rev. **104** (2004) 5005, and references their in.
- 3) H. Kino and H. Kontani: J. Phys. Soc. Jpn. **67** (1998) 3691.
- 4) H. Kondo and T. Moriya: J. Phys. Soc. Jpn. **67** (1998) 3695.
- 5) M. Vojita and E. Dagotto: Phys. Rev. B. **59** (1999) R713.
- 6) T. Jujo, S. Koikegami and K. Yamada: J. Phys. Soc. Jpn. **68** (1999) 1331.
- 7) A. Kobayashi, S. Katayama, K. Noguchi and Y. Suzumura: J. Phys. Soc. Jpn. **73** (2004) 3135.
- 8) A. Kobayashi, S. Katayama and Y. Suzumura: J. Phys. Soc. Jpn. **74** (2005) 2897.
- 9) H. Seo: J. Phys. Soc. Jpn. **69** (2000) 805.
- 10) M. Kaneko and M. Ogata: J. Phys. Soc. Jpn. **75** (2006) 14710.
- 11) Y. Tanaka, Y. Yanase and M. Ogata: J. Phys. Soc. Jpn. **73** (2004) 2053, and references their in.
- 12) S. Kimura, H. Suzuki, T. Maejima, H. Mori, J. Yamaura, T. Kakiuchi, H. Sawa and H. Moriyama: J. Am. Chem. Soc. **128** (2006) 1456.
- 13) S. Kimura, T. Maejima, H. Suzuki, R. Chiba, H. Mori, T. Kawamoto, T. Mori, H. Moriyama, Y. Nishio and K. Kajita: Chem. Commun. (2004) 2454.
- 14) H. Mori: J. Phys. Soc. Jpn. **75** (2006) 051003.
- 15) D. Jaccard, K. Behnia and J. Sierro: Phys. Lett. A **163** (1992) 475.
- 16) N. D. Mathur, F. M. Grosche, S. R. Julian, I. R. Walker, D. M. Freye, R. K. W. Haselwimmer and G. G. Lonzarich: Nature **394** (1998) 39.
- 17) S. S. Saxena, P. Agarwal, K. Ahilan, F. M. Grosche, R. K. W. Haselwimmer, M. J. Steiner, E. Pugh, I. R. Walker, S. R. Julian, P. Monthoux, G. G. Lonzarich, A. Huxley, I. Sheikin, D. Braithwaite and J. Flouquet: Nature **406** (2000) 587.
- 18) T. Yamauchi, Y. Ueda and N. Mori: Phys. Rev. Lett. **89** (2002) 057002.
- 19) M. Tamura and R. Kato: J. Phys. Soc. Jpn. **73** (2004) 3108.
- 20) A. Kobayashi, Y. Tanaka, M. Ogata and Y. Suzumura: J. Phys. Soc. Jpn. **73** (2004) 1115.
- 21) N. Tajima, A. E. Tajima, M. Tamura, Y. Nishio and K. Kajita: J. Phys. Soc. Jpn. **71** (2002) 1832.